Intraoperative High-Field Magnetic Resonance Imaging Combined With Fiber Tract Neuronavigation-Guided Resection of Cerebral Lesions Involving Optic Radiation

Guo-chen Sun, MD*‡
Xiao-lei Chen, MD, PhD*‡
Yan Zhao, MD‡
Fei Wang, MD‡
Bao-ke Hou, MD§
Yu-bo Wang, MD‡
Zhi-Jun Song, MD‡
Dong Wang, MD‖
Bai-nan Xu, MD, PhD‡

Departments of ‡Neurosurgery, §Ophthalmology, and ‖Radiology, PLA General Hospital, Beijing, China

*These authors have contributed equally to this article.

Correspondence:
Bai-nan Xu,
Department of Neurosurgery,
PLA General Hospital,
28 Fuxing Rd,
Beijing, 100853, China.
E-mail: sjwk301@Gmail.com

Received, October 19, 2010.
Accepted, March 25, 2011.
Published Online, June 7, 2011.

BACKGROUND: Intraoperative magnetic resonance imaging (iMRI) combined with optic radiation neuronavigation may be safer for resection of cerebral lesions involving the optic radiation.

OBJECTIVE: To investigate whether iMRI combined with optic radiation neuronavigation can help maximize tumor resection while protecting the patient's visual field.

METHODS: Forty-four patients with cerebral tumors adjacent to the optic radiation were enrolled in the study. The reconstructed optic radiations were observed so that a reasonable surgical plan could be developed. During the surgery, microscope-based fiber tract neuronavigation was routinely implemented. The lesion location (lateral or not to the optic radiation) and course of the optic radiation (stretched or not) were categorized, and their relationships to the visual field defect were determined.

RESULTS: Analysis of the visible relationship between the optic radiation and the lesion led to a change in surgical approach in 6 patients (14%). The mean tumor residual rate for glioma patients was 5.3% (n = 36) and 0% for patients with nonglioma lesions (n = 8). Intraoperative MRI and fiber tract neuronavigation increased the average size of resection (first and last iMRI scanning, 88.3% vs 95.7%; $P < .01$). Visual fields after surgery improved in 5 cases (11.4%), exhibited no change in 36 cases (81.8%), and were aggravated in 3 cases (6.8%).

CONCLUSION: Diffusion tensor imaging information was helpful in surgical planning. When iMRI was combined with fiber tract neuronavigation, the resection rate of brain lesions involving the optic radiation was increased in most patients without harming the patients' visual fields.

KEY WORDS: Diffusion tensor imaging, Intraoperative MRI, Neuronavigation, Optic radiation, Visual field

Neurosurgery 69:1070–1084, 2011 DOI: 10.1227/NEU.0b013e3182274841 www.neurosurgery-online.com

The optic radiation is a group of axons from relay neurons in the lateral geniculate nucleus of the thalamus that carry visual information to the visual cortex. It was first described and identified in 1856 by Louis Pierre Gratiolet.[1] The ability to accurately describe the course and extent of the optic radiation in vivo is important for studies relating its structure to its function. Relying on the Klingler method of white matter fiber dissection, several researchers[1-5] performed studies to improve the understanding of the morphological characteristics of the optic radiation and to give a better interpretation of the complex relationships of these myelinated fascicles.

Optic radiation infiltration or destruction can be induced by lesions or by neurosurgeons who try to resect lesions adjacent to the tract and thereby inadvertently damage the fiber tract. Although some anatomical landmarks have been ascertained that are helpful in predicting the localization of the optic radiation, the risk of optic radiation damage seems unavoidable

ABBREVIATIONS: DTI, diffusion tensor imaging; **iMRI,** intraoperative magnetic resonance imaging; **VOI,** volume of interest

because the optic radiation is not visible under the naked eye or microscope.[1,4-9] However, in lesions close to or near the optic radiation, the normal anatomic location and shape of the optic radiation change; thus, it is sometimes not possible to distinguish the traditional anatomic landmarks. In addition, normal anatomic variations in the optic radiation lead to poor reliability in the use of anatomic landmarks.

Diffusion tensor imaging (DTI) enables visualization and characterization of white matter fiber tracts.[10-14] Since the introduction of this methodology in 1994,[15] it has been used to study white matter architecture and the integrity of normal and diseased brains. This magnetic resonance technique is based on the general principle that the diffusion of water is directed by the anatomic microstructure. White matter fiber orientation can be determined by using DTI because water diffuses faster parallel to the longitudinal axis of axons than perpendicular to it.[15] The directional information may be simply visualized with the color-coded maps representing the major direction. These color-coded maps are very useful for investigating the organization and course of white matter in the brain and for identifying major white matter tracts in 2-dimensional sections.[16-21] However, the 2-dimensional pattern cannot be visualized during surgery and cannot be used for functional neuronavigation. Another approach for appreciating the white matter connection patterns in 3 dimensions (3D) is the use of fiber tracking, also known as tractography, which follows coherent spatial patterns in the major direction of the diffusion tensor field.[22-26]

So far, fiber tracking is the only noninvasive method for visualizing the course, displacement, or interruption of major white matter tracts based on the DTI technique.[27-31] Multiple studies have demonstrated that fiber tracking can reconstruct the major white matter fiber structures in the brain. In our previous study,[32] we used DTI-based fiber tracking for the detection and localization of the optic radiation for temporal lobectomy, and we verified the validity and the repeatability of the technique. A few studies with very small cohorts of patients have demonstrated the effects of surgery on lesions adjacent to the optic radiation.[33-37] It has not yet been established whether intraoperative magnetic resonance imaging (iMRI) combined with neuronavigation-guided resection of cerebral lesions involving the optic radiation could help protect the patient's visual field.

In the present prospective study, we sought to evaluate the possibility of identifying the trajectories of the optic radiation when a lesion is located adjacent to it, to examine the usefulness of a neuronavigation system for presurgical planning, and to investigate whether iMRI combined with integrated neuronavigation can help maximize tumor resection while protecting the patient's visual field.

MATERIALS AND METHODS

Patient Population

Forty-four patients with cerebral lesions adjacent to the optic radiation (the patient who had a lesion involving the primary optic cortex was excluded from the study) were consecutively and prospectively enrolled in our study. All patients were operated on with iMRI and neuronavigation between March 2009 and January 2010. Of the 44 patients, 29 were male and 15 were female. The average age of the patients in the study cohort was 40.9 years (SD = 14.4 years; range, 14-68 years). All patients underwent tailored craniotomy to resect the lesion. Patient data are listed in Table 1.

Conventional anatomical MRI (T1, T2, and T2 flair and postcontrast images [sometimes magnetic resonance angiography, magnetic resonance venogram, and magnetic resonance spectroscopy]) and DTI data were prospectively collected. All patients had preoperative, intraoperative, and postoperative MRI and preoperative and postoperative visual field examination (3 months after surgery). We excluded those patients who presented with other ophthalmic or neurological causes of visual field defects. The local ethics committee of the hospital approved intraoperative MRI, and signed informed consent was provided by all patients or family members.

Image Acquisition (Preoperative and Intraoperative Imaging)

Both conventional MRI and DTI were performed on a 1.5-T scanner (Siemens Espree, Erlangen, Germany) following the same protocol. A T1-weighted 3D magnetization-prepared rapid-acquisition gradient echo sequence was measured with an echo time of 3.02 milliseconds, a repetition time of 1650 milliseconds, a matrix size of 256 × 256, a field of view of 250 × 250 mm, a slice thickness of 1 mm, and a slab of 16 cm. In addition, T2-weighted images (echo time, 93 milliseconds; repetition time, 5500 milliseconds; matrix size, 512 × 512; field of view, 230 × 230 mm; slice thickness, 3 mm), T2 fluid-attenuated inversion recovery images (echo time, 84 milliseconds; repetition time, 9000 milliseconds; matrix size, 256 × 256; field of view, 230 × 230 mm; slice thickness, 3 mm), and postcontrast 3D T1-weighted images were scanned. Intraoperative scans were performed immediately when the operator believed that the lesion has been totally removed or when intraoperative scanning was necessary for brain shift correction.

For DTI, we applied a single-shot spin-echo diffusion-weighted echo-planar imaging sequence (echo time, 147 milliseconds; repetition time, 9400 milliseconds; matrix size, 128 × 128; field of view, 251 × 251 mm; slice thickness, 3 mm; bandwidth, 1502 Hz per pixel; diffusion-encoding gradients in 12 directions using b values of 0 and 1000 s/mm^2; and voxel size, 1.9 × 1.9 × 3 mm). We used 40 slices, no intersection gap, 40 continuous free interval collection slices, and 5 time repetitions. The total scan time was 10 minutes 22 seconds).

Image Processing (Tractography)

Before fiber tracking can be started, format conversion of the data and infusion of the different sets of images are needed. For fiber tracking, we implemented a tracking algorithm based on a tensor deflection algorithm. Generally, the course of a fiber is defined by following the direction of maximum diffusion. We used the fiber tracking module of the neuronavigation planning software iPlan 2.6 (BrainLab, Feldkirchen, Germany) to reconstruct the optic radiation. Fiber tracking was performed by the first author while blinded to the results of the patient's visual field. Details of the method have previously been published.[4] Before tracking was initiated, the fractional anisotrophy threshold was adjusted to 0.15, the angle threshold to 20. and the minimum fiber length to 50 mm (stop criteria). Tract seeding was performed by defining a rectangular volume of interest (VOI) in the coregistered standard T1 anatomic data sets. We used a multi-VOI algorithm for fiber tracking of

TABLE 1. Patient Characteristics, Lesion Location/Volumes, Lesion-to-Optic-Radiation Distance, Visual Field, and Relationship Between the Lesion and Optic Radiation[a]

Patient	Age, y	Sex	PD	Location	Side	Lesion Volume, cm^3	Intention of Extent of Resection	Estimation of Extent of Resection Before the First iMRI	Actuality of Extent of Resection After the First iMRI
1	64	F	IV	Temporal-occipital	R	41.7	100	90	83
2	57	M	IV	Temporal	R	56.6	100	100	100
3	55	M	III	Temporal-parietal	R	58.8	100	95	100
4	31	F	II	Parietal-occipital	L	31.1	60	90	56.9
5	46	M	AVM	Temporal	L	63.3	100	100	100
6	31	M	II	Parietal-occipital	L	48.7	90	95	97.9
7	55	M	IV	Temporal-insular	L	2.3	100	100	100
8	36	F	II	Temporal	R	16.1	100	100	100
9	64	F	IV	Temporal	L	38.7	90	90	100
10	24	M	II	Temporal	L	36.1	100	100	100
11	27	M	IV	Temporal	L	29.6	100	98	70.6
12	62	M	IV	Temporal	R	5.5	100	100	100
13	35	F	II	Parietal	L	22.8	60	40	45.2
14	38	M	II	Temporal-occipital	R	84.6	100	100	100
15	25	M	II	Temporal-insular	R	85.2	100	80	75.4
16	17	M	II	Frontal-temporal	L	58.2	100	100	100
17	57	M	II	Temporal-parietal	R	45.1	100	100	90
18	40	F	CH	Temporal	R	2.1	100	100	100
19	45	M	IV	Temporal	R	74.7	70	70	90
20	54	F	II	Temporal	R	40	60	60	60
21	34	F	II	Temporal-insular	R	44.6	90	90	95.1
22	57	M	IV	Temporal	L	64.5	90	90	89.3
23	35	M	IV	Temporal	R	110.2	90	80	62.7
24	55	M	II	Frontal-temporal	R	29.9	60	50	55.9
25	24	F	II	Temporal	R	15.6	100	99	85.9
26	39	M	II	Temporal	L	16.5	100	100	100
27	58	F	MT	Parietal	R	13.7	100	100	100
28	29	M	III	Frontal-temporal-insular	R	110.5	90	80	70
29	20	M	II	Temporal-insular	L	35.2	90	60	69.9
30	14	F	I	Temporal-insular	R	60.3	100	100	94.4
31	44	F	IV	Frontal-temporal	L	35.6	100	100	100
32	38	M	II	Parietal	L	53.4	90	80	77.3
33	68	M	III	Temporal	R	76.4	60	60	55.5
34	40	M	IV	Parietal-occipital	R	53.9	90	95	89.2
35	21	M	I	Temporal	R	4.6	100	100	100
36	42	F	CH	Temporal	R	3.5	100	100	100
37	36	M	CH	Temporal	R	2.3	100	100	100
38	45	M	CH	Temporal	R	3.4	100	100	100
39	23	F	CH	Temporal-parietal	R	9.4	100	100	100
40	55	M	II	Temporal	L	52.9	90	95	93.8
41	20	M	II	Parietal-occipital	L	46.5	90	95	81.4
42	46	M	II	Temporal	R	5.3	100	100	96.2
43	51	F	MT	Temporal	L	12.7	100	100	100
44	43	M	II	Temporal	R	34.1	100	100	100

(Continues)

the optic radiation. For the ventral bundle of the optic radiation (the Meyer loop), the first VOI was placed on the lateral geniculate body. The second VOI was placed to cover the lower lip of the visual occipital cortex (calcarine cortex). We identified the lateral geniculate body by selecting the axial slice at the level of the transition from the posterior limb of the internal capsule to the cerebral peduncle. At this level, the lateral geniculate body is visible posterolateral to the peduncle. For reconstructing the dorsal bundle of the optic radiation (central and posterior bundle), the first VOI was also placed on the lateral geniculate body, and the second VOI was placed to cover the middle and upper lip of the visual

TABLE 1. ***Continued***

Patient	Residual Lesion Volume After the First iMRI	Residual Lesion Volume After the Final iMRI	Times of iMRI	Lesion to OR Distance, mm	Preoperative Visual Field	Postoperative Visual Field	Change in Visual Field	Lateral Location of the Lesion to OR or Not	OR Was Stretched by the Lesion or Not
1	7.1	0	2	0.0	1	1	2	1	0
2	0	0	1	0.0	2	0	1	0	0
3	0	0	1	0.0	1	2	3	1	1
4	12.4	6.2	2	1.9	1	1	2	1	0
5	0	0	1	1.5	0	0	2	0	0
6	1	0	2	0.0	1	1	2	0	1
7	0	0	1	5.6	0	0	2	0	0
8	0	0	1	2.4	0	0	2	0	0
9	0	0	1	2.7	1	1	2	1	1
10	0	0	1	5.5	0	0	2	0	0
11	8.7	3.2	2	3.6	1	1	2	0	0
12	0	0	1	1.2	1	1	2	1	0
13	12.5	3	3	0.9	1	0	1	0	0
14	0	0	1	0.0	2	1	1	0	0
15	21	0	3	7.5	0	0	2	0	0
16	0	0	1	7.1	0	0	2	0	0
17	4.5	0	2	3.5	1	0	1	0	0
18	0	0	1	1.9	1	1	2	1	0
19	7.5	7.5	1	14.0	0	0	2	0	0
20	15.6	8.7	2	0.9	0	0	2	1	0
21	2.2	2.2	1	3.3	0	0	2	1	1
22	6.9	6.9	1	0.0	0	0	2	1	0
23	44.1	11	2	0.0	0	0	2	1	1
24	13.2	0	2	0.0	0	2	3	1	1
25	2.2	0	2	1.0	0	0	2	0	0
26	0	0	1	11.8	0	0	2	1	0
27	0	0	1	6.1	0	0	2	0	0
28	33.2	22.1	2	1.8	0	0	2	0	0
29	10.6	2.8	2	2.3	0	0	2	0	1
30	3.6	0	3	3.4	0	0	2	0	0
31	0	0	1	6.3	0	0	2	1	0
32	9.1	5.3	2	3.7	0	0	2	0	0
33	30.6	30.6	1	0.0	1	1	2	1	0
34	5.4	0	2	0.0	1	2	3	1	1
35	0	0	1	6.7	0	0	2	0	0
36	0	0	1	6.5	0	0	2	0	0
37	0	0	1	2.6	0	0	2	0	0
38	0	0	1	3.1	0	0	2	0	0
39	0	0	1	0.0	1	0	1	0	0
40	2.6	2.6	1	6.3	0	0	2	0	0
41	8.6	0	2	0.0	1	1	2	1	1
42	0.2	0.2	1	0.0	1	1	2	1	0
43	0	0	1	4.9	0	0	2	1	0
44	0	0	1	4.8	0	0	2	0	0

[a]CH, cavernous hemangioma; iMRI, intraoperative magnetic resonance imaging; I to IV glioma, World Health Organization grade I to IV; MT, metastatic tumor; OR, optic radiation; PD, pathological diagnosis. For visual field examination, the scores were as follows: 0 = no deficit; 1 = quadrantanopia; 2 = hemianopia. The change in the visual field is given as follows: 1 = improved; 2 = not change; 3 = aggravated. The location of the optic radiation to the lesion was scored as 0 = anterior, rostral or caudal or 1 = medial or lateral. The optic radiation was stretched (1) or not (0).

occipital cortex. The fiber tract that passed through both VOIs was the final tract of interest. After selection of the appropriate fiber bundle, a 3D object was "created" automatically by wrapping neighboring fibers with a hull. The closing lines around all fibers from all slices together result in the 3D object. The time required to process the DTI data and to acquire the 3D object was approximately 10 minutes (sometimes the pyramidal tracts and arcuate fasciculus were also "created" when needed when the relevant data were under collection).

For segmentation of image data for 3D reconstruction of tumor, we used the object creation module of the iPlan 2.6. Tumor segmentation was performed on the basis of the high-resolution postcontrast 3D anatomic data set. The outermost rim of contrast enhancement in the lesion, eg, glioblastoma and metastatic tumors, and the rim of the mixed hyperintensity or hypointensity in the lesion such as cavernoma represented the segmentation borderline. In the case of nonenhanced lesions such as low-grade glioma, the T2-weighted image was used to determine the tumor border. This reason was that the majority of the tumor, which was not contrast enhanced, has optimal visibility in this sequence. The existence of a substantial edema, which could not be distinguished clearly from low-grade glioma, was ruled out on the basis of the findings from T2 fluid-attenuated inversion recovery images. Segmentation of the tumor was performed on a slice-by-slice basis in a mode of 3D anatomic data. After all the slices containing the lesion were outlined, the lesion was formed into a 3D object, and the volume was automatically calculated by computer. The minimum distance between the optic radiation and the lesion was measured with the object manipulation function of the iPlan 2.6. Relative to the lesion, the location of the optic radiation was categorized as lateral, medial, anterior, rostral, or caudal. When the optic radiation was pushed 10 mm by the lesion, we recognized that the tract was stretched.

Preoperatively, the conventional MRI was evaluated by the neurosurgery group and then was integrated with the 3D fiber tract, and the lesion was revealed. Neurosurgeons were asked whether the tractography images had modified the access or approach to the tumor.

Microscope-Based Neuronavigation

For anatomic neuronavigation, the 3D postcontrast T1-weighted sequence was used for intraoperative imaging. Functional data from DTI or functional MRI used to identify eloquent brain areas such as optic radiation and visual cortex were integrated in selected cases into the 3D image data. Details of these techniques have been published elsewhere.[38-40] After the patient was registered accurately, the neuronavigation microscope (Pentero, Carl Zeiss, Oberkochen, Germany) was connected. The contour of the lesion and the functional data were overlaid in the neurosurgeon's microscope viewing field.

Updating Neuronavigation With Intraoperative Image Data

Intraoperative brain shift can be caused by tumor resection, brain swelling, use of brain retractors, and cerebrospinal fluid runoff. Thus, a neuronavigation system that is based on preoperative imaging data will have decreasing accuracy during the operation. Intraoperative imaging offers the possibility of compensating for brain shift and evaluating how much tumor is removed. The location of the optic radiation can also be updated by fiber tracking.

Visual Field Examination

The patients underwent visual field examination both preoperatively and postoperatively. Visual field analysis was performed with a Humphrey Field Analyser II (Carl Zeiss, Meditec, Japan) by an experienced ophthalmologist who was blinded to the results of the neuroimaging findings. All postoperative visual field examinations were carried out 3 months after the surgery.

Statistics

Statistical analyses were performed with the Statistical Package for the Social Sciences software (version 14.0; SPSS, Inc, Chicago, Illinois). The Student t test was used to evaluate the average rate of extent of resection between the first and last iMRI scannings. Spearman rank correlation analysis was used to assess correlations between the deterioration of visual field and the lateral location or not of the optic radiation and whether it was stretched. A value of $P \leq .05$ was considered statistically significant.

RESULTS

Impact of DTI on Surgical Planning

Fiber bundles representing the optic radiation could be generated both preoperatively and intraoperatively in all patients. The preoperative DTI information on the optic radiation was adopted to assess the practical impact on surgical planning. In 6 cases, the surgical approach was changed when the DTI information was shown to surgeon groups after conventional MRI. The original approach provides the shortest trajectory to the lesion while avoiding disruption of the imaginary visual fiber location. However, the reconstructed optic radiation was in the way of access to the lesion if the original approach would have been adopted, which would most likely cause injury to optic radiation. The final selected approach was chosen on the basis of information on the relationship between the segmented lesion and the reconstructed optic radiation. Finally, none of these 6 patients had postoperative visual field deterioration (Table 2).

Discrepancy Between the Surgeon's Estimation of the Extent of the Resection and Actual Results

There was a discrepancy between the surgeon's estimation regarding the extent of the resection before iMRI scanning and the actual results of surgery assessed after the first iMRI. Of the 9 discrepant (a gap $\geq$ 10%) patients, all were glioma patients: 8 patients (4 with low-grade glioma and 4 with high-grade glioma) were overestimated and 1 patient with high-grade glioma was underestimated. The surgeon tended to overestimate the extent of the resection.

Impact of the iMRI on the Extent of Resection

There were 36 patients with gliomas: 22 with low-grade gliomas and 14 with high-grade gliomas. The preoperative median tumor volume was 45.2 cm^3 (range, 2.3-110.5 cm^3); the mean lesion to optic radiation distance was 3.0 $\pm$ 3.5 mm (median, 2.1 mm; range, 0-14 mm), with a final mean tumor residue of 5.3% (range, 0%-40%) after surgery. In all patients, iMRI was performed at least once. The first intraoperative imaging demonstrated incomplete tumor resections in 23 patients (63.9%) and gross total tumor resections in 13 patients (36.1%). In 19 patients in whom surgery was terminated after the first iMRI, in 6 of the 19 patients with incomplete tumor removal, further resection was abandoned owing to postoperative visual field deterioration expected if resection was continued. This included 3 patients with World Health Organization grade II tumor, 1 with grade III tumor, and 2 with grade IV tumor. In 17 patients with at least partially resectable residual tumors revealed by the first intraoperative scan, further tumor

TABLE 2. Patients Whose Original Approach Was Changed After the Reconstructed Optic Radiation Was Shown to the Surgeon Groups[a]

Patient	Pathological Diagnosis, WHO Grade Glioma	Location of the Lesion	Side	Original Approach	Final Elected Approach
6	II	Parietal-occipital lobe	Left	Triangle transcortical	High occipital transcortical
41	II	Parietal-occipital lobe	Left	Superior temporal gyrus	Occipital interhemispheric
23	IV	Temporal lobe	Right	Triangle transcortical	High occipital transcortical
20	II	Temporal lobe	Right	Triangle transcortical	Occipital interhemispheric
8	II	Temporal lobe	Right	Middle temporal gyrus	Transsylvian fissure
10	II	Temporal lobe	Left	Middle temporal gyrus	Inferior temporal gyrus

[a]WHO, World Health Organization.

resections were continued after updating the neuronavigation. In these 17 patients (12 low-grade gliomas and 5 high-grade gliomas) of the 36 patients who underwent continued resection, iMRI was repeated once in 14 patients and twice in 3 patients. As a result, total tumor removal was achieved in 9 of the 17 patients (52.9%). However, to avoid damage to the optic radiation, only partial tumor removal was carried out in the remaining 8 patients (47.1%). Attributed to further tumor resection, the average resection rate increased from 74.5% to 93.3% ($P < .01$). There was a significant correlation between tumor to optic radiation distance and tumor residue after the first iMRI ($r = 0.380$, $P < .05$). However, there was no significant correlation between tumor to optic radiation distance and the final extent of resection after further resection ($r = 0.232$, $P > .05$). Finally, 22 patients (61.1%) had total tumor removal. The iMRI and functional neuronavigation also contributed to an increase in the average rate of resection in glioma patients (first and last iMRI scannings, 85.7% vs 94.7%; $P < .01$, Student t test).

In the 8 patients with nongliomas (1 arteriovenous malformation, 5 cavernous hemangiomas, and 2 metastatic tumors), the preoperative mean lesion volume was 13.8 cm^3 (range, 2.1-63.3 cm^3) and the mean lesion to optic radiation distance was 3.3 $\pm$ 2.3 mm (median, 2.9 mm; range, 0-6.5 mm), with no lesion residual after the first iMRI (Table 1 and Figure 1).

The Visual Field Examination Outcome

In the total population of 44 patients, compared with preoperative levels, visual field defects were improved after surgery in 5 patients (11.4%), visual fields were unchanged in 36 patients (81.8%), and visual fields were aggravated in 3 patients (6.8%).

In the 36 glioma patients, there were 27 patients in whom the distance from the lesion to the optic radiation was < 5 mm, 12 patients had normal visual field, and 15 patients had various degrees of preoperative visual field defects (13 patients had quadrantanopia and 2 patients had hemianopia). Postoperatively, the visual fields were normal in 14 patients, 10 patients had quadrantanopia, and 3 patients had hemianopia. The visual fields improved in 4 patients, were unchanged in 20 patients, and deteriorated in 3 patients; all 9 patients in whom the distance from the lesion to the optic radiation was > 5 mm had preoperative and postoperative normal visual field. As for the 3 patients with deteriorated visual field, 2 had preoperative visual field defects and 1 had a normal preoperative visual field in which the distance between the lesion and the optic radiation was < 5 mm; 1 patient was in the group who were terminated after the first iMRI, and 2 patients were in the further resection group.

In the 8 nonglioma patients, there were no patients with postoperative visual field defect deterioration. One patient had preoperative quadrantanopia caused by hemorrhage of the cavernous hemangioma; postoperatively, the visual field recovered to normal. Another patient with a lesion (cavernous hemangioma) to optic radiation distance of 0 mm had preoperative quadrantanopia; postoperatively, the visual field showed no change from the preoperative examination. The other 6 patients in this group had both preoperative and postoperative normal visual field.

Decreasing lesion to optic radiation distance was a negative factor for visual field preservation ($P < .05$). Spearman rank correlation analysis showed that the deterioration of visual field was also related to tract stretching ($r = 0.446$, $P < .01$) and lateral localization ($r = 0.415$, $P < .01$).

ILLUSTRATIVE CASE

Case 1

A 24-year-old female patient (patient 25) suffered from a headache for 2 weeks. Preoperative MRI showed a nonenhanced lesion in the right temporal lobe (Figures 2A-2E). The diagnosis, based on conventional MRI and MR spectroscopy, was low-grade glioma. Preoperative DTI-based fiber tracking showed that the Meyer loop was rostral to the lesion and was pushed slightly upward. The minimum distance between the lesion and the optic radiation was approximately 1.0 mm (Figure 2C-2G). Preoperative visual field examination showed it to be normal. A right middle temporal approach was planned on the basis of the 3D relationship between the lesion and the optic radiation (Figure 2H). According to neuronavigation, a suitable cortex incision was designed (Figure 3A). To better protect the Meyer loop, we created a 5-mm hull (the outer blue line in Figure 3A and 3B). During the operation, when the dotted line delineating the hull turned into a solid line, the surgeon was reminded that

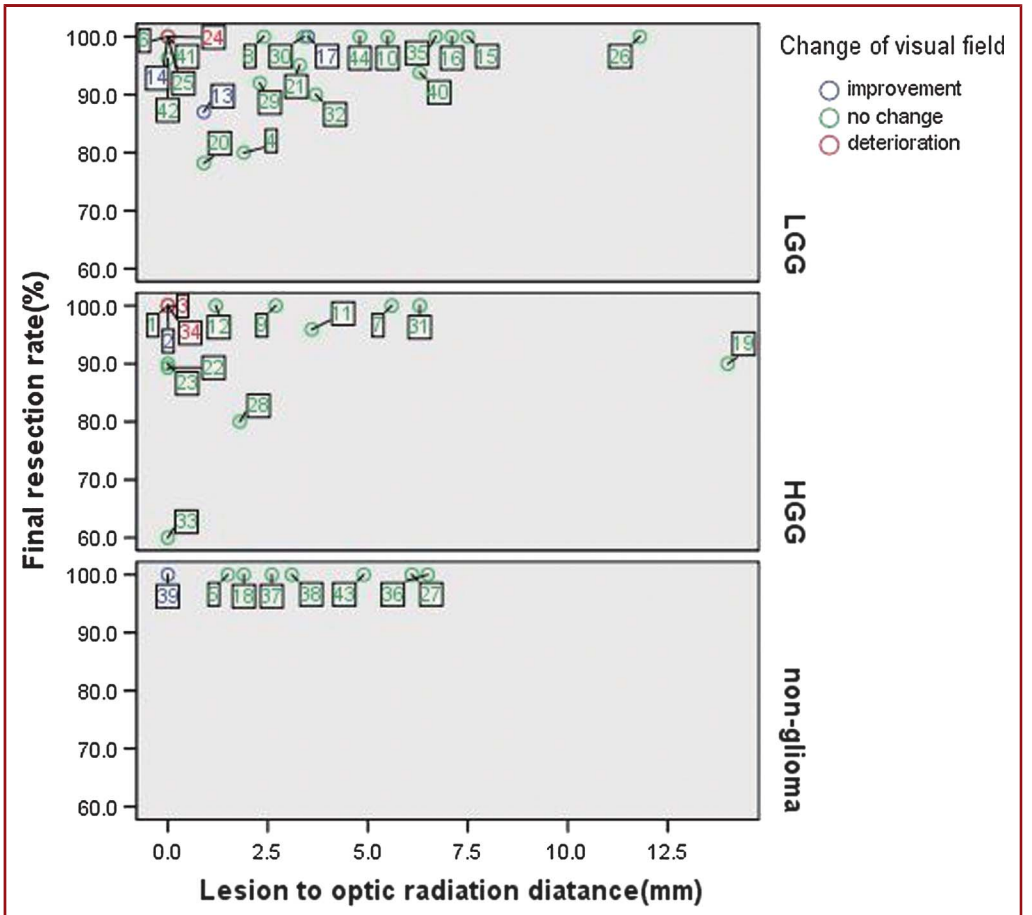

FIGURE 1. *Lesion to optic radiation distance plotted vs the extent of resection and change of visual field for patients with low-grade gliomas (LGGs) and high-grade gliomas (HGGs) and nonglioma patients. One patient with an LGG and 2 patients with HGGs had an aggravated postoperative visual field; all of them were in the total removal group and with a lesion to optic radiation distance of 0 mm. All the nonglioma patients had total tumor removal without deterioration of visual fields.*

the manipulation was close to the optic radiation (microscope video in Figure 3B). Subsequently iMRI was performed and revealed that a partial lesion remained after surgery. Intraoperative DTI-based fiber tracking revealed that the Meyer loop can be accurately traced (Figure 3D-3F). After we infused the intraoperative optic radiation tractography on the intraoperative image and outlined the residual tumor, the neuronavigation was updated, microscope-based navigation helped locate the residual lesion accurately, and further resection of the lesion continued (Figure 3C). Final intraoperative scanning revealed that the tumor had been totally removed (Figures 2F and 3G-3I). The pathological diagnosis was World Health Organization grade II astrocytoma. According to the imaging findings at 3 months after surgery, the Meyer loop was completely preserved and the lesion was totally removed (Figure 4A-4D). Perimetry examination at 3 months after the operation revealed no visual field defects.

DISCUSSION

Diffusion tensor imaging has become one of the most popular MRI techniques for studying the brain and associated clinical applications.[18,41-44] Diffusion tensor imaging enables visualization and characterization of white matter tracts in 3D.[45-47] Recently, fiber tracking has been used for preoperative visualization of white matter tracts in patients with space-occupying lesions.[48-53] The concept of integrating functional data from functional MRI into anatomic 3D data sets has been widely used for preoperative neurosurgical planning and for intraoperative identification of eloquent structures and is known as functional neuronavigation.[54,55] In our previous study, we were the first group to present a study that evaluated the feasibility, accuracy, and validity of DTI-based fiber tracking of the optic radiation. The bundles of the optic radiation that were depicted agreed well

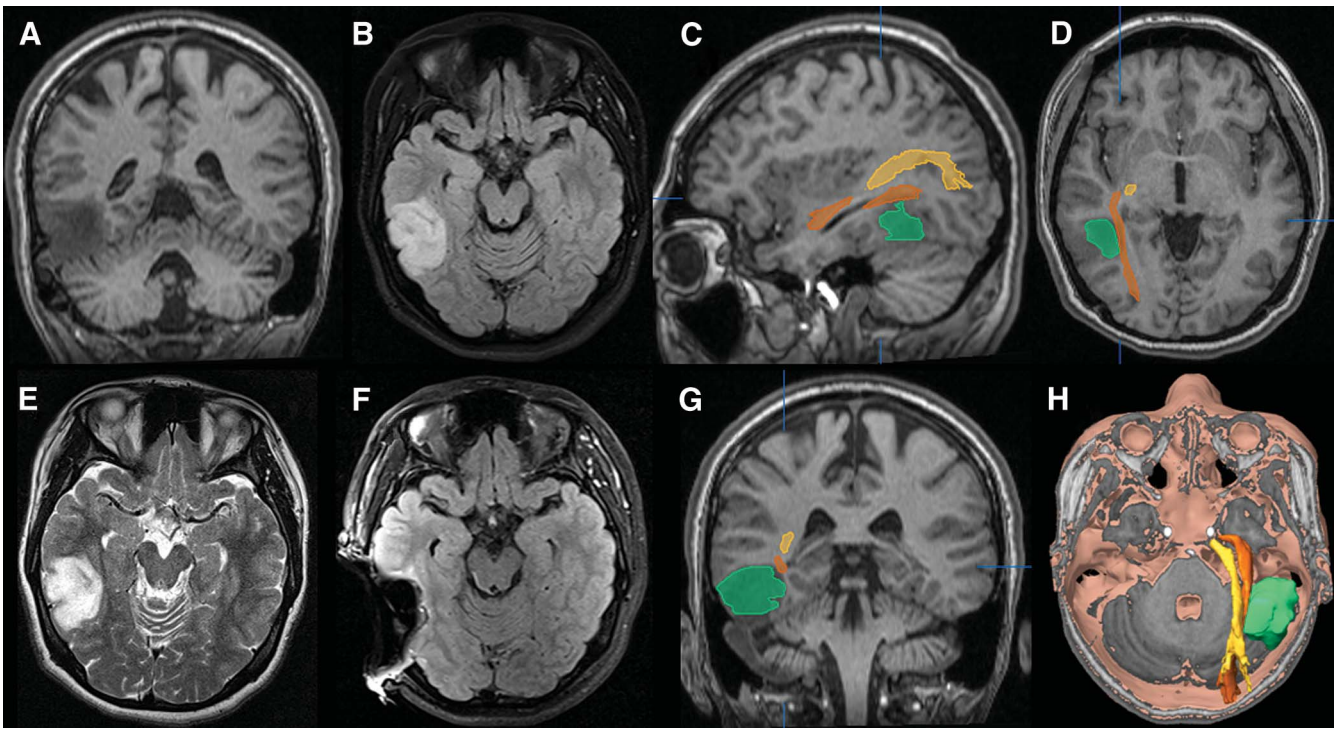

FIGURE 2. *A 24-year-old female patient (patient 25) presented with headache. Conventional MRI showed a glioma located in the right temporal lobe; the lesion revealed a long T1 (**A**) and a long T2 (**E**) signal. The preoperative and final intraoperative T2 fluid-attenuated inversion recovery images are shown in **B** and **F**. The reconstructed Meyer loop was rostral to the lesion, and the minimum distance between the lesion and the optic radiation was approximately 1.0 mm (**C**, **D**, and **G**; yellow, dorsal bundle; brown, the Meyer loop). The 3D relationship between the lesion and the optic radiation is shown in **H**.*

with the classic theory of anatomic topography of the visual pathway. Our findings were also consistent with the findings of modern dissection and MRI studies. In the present study, the optic radiation in all patients could be successfully reconstructed. As for the surgical planning, the surgical approach changed in 6 patients after the optic radiation information was shown to the surgeon groups, for the original approach would have inevitably destructed the vital tract. The visual fields maintained well after surgery in these 6 patients.

As has been reported, DTI-based fiber tracking can be implemented as a neuronavigation system, making it possible to visualize the course of the major white matter tracts intraoperatively.[54,56] However, there have been few small cohort reports concerning optic radiation-guided surgery.[9,11,33] The present study was implemented on the optic radiation using a microscope-based neuronavigation. Sometimes, total removal of the lesion may be in conflict with the preservation of the optic radiation. However, at least preoperative DTI should be useful in better estimating the risk of visual field defects, so that the most appropriate surgical approach and surgical procedure can be chosen to minimize neurological deficit. Additionally, preoperative DTI allows the risks to be discussed in greater detail with the patients and relatives before surgery.

Intraoperative MRI combined with neuronavigation has proved to be a safe technique that enables the neurosurgeon to update data sets for neuronavigation, to evaluate the extent of tumor resection, to correct for brain shift, to modify surgery if necessary, to guide instruments to the site of the lesion, and to evaluate the presence of intraoperative complications at the end of surgery.[57] Intraoperative high-field MRI with integrated microscope-based neuronavigation is at present one of the most well-developed technical methods, providing a reliable and immediate intraoperative quality evaluation.[58-60] We investigated the contribution of iMRI in reducing the final residual tumor volume with further resection while protecting the optic radiation. During the operation, intraoperative visualization of the optic radiation adjacent to the tumor contour facilitated preservation of this eloquent brain structure. The display of contours in the microscopic surgical field gave a very intuitive 3D impression of the actual course of the optic radiation, so that the surgeons were able to maximize the resection while maintaining the integrity of the optic radiation. When the preset tumor border was reached or the dotted line turned into solid line in the microscope field, the surgeon stopped manipulation and obtained an iMRI scan. The intraoperative image data could be used for immediate visualization of the shifted optic radiation relative to the resection cavity

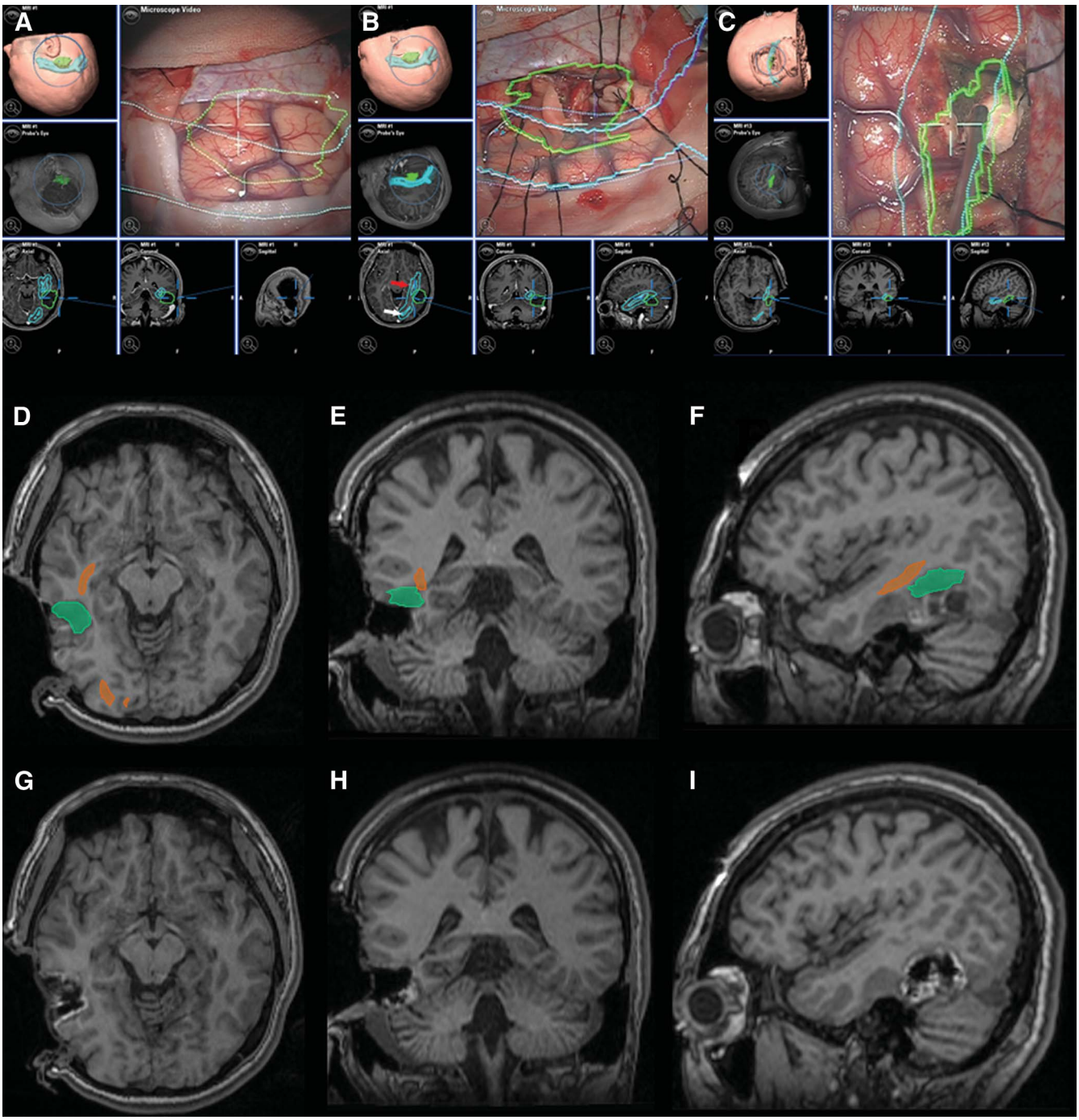

FIGURE 3. *From the microscope-based neuronavigation, we can accurately determine where to incise the cortex (**A**). To better protect the Meyer loop (white arrow), we created a 5-mm hull for it (outer blue line in **A** and **B**, marked by a red arrow). During the operation, when the dotted line delineating the hull turned into a solid line, the surgeon was reminded that the manipulation was close to the optic radiation and an intraoperative MRI was necessary (microscope video in **B**). The first intraoperative MRI demonstrated that the partial lesion near the optic radiation remained (**D**-**F**). The neuronavigation was updated; microscopic-based navigation helped to locate the residual lesion accurately; and further resection of the lesion continued (**C**). Final intraoperative scanning revealed that the tumor had been nearly totally removed (**G**-**I**).*

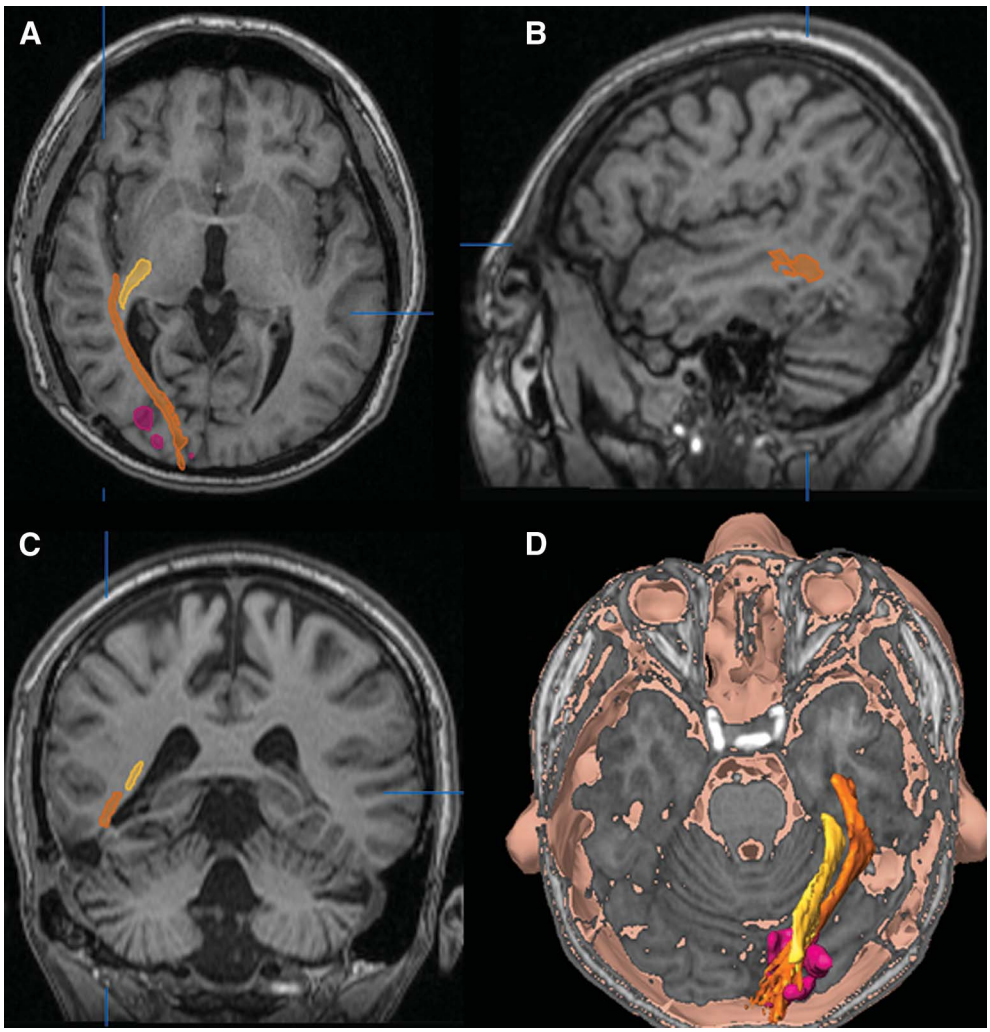

FIGURE 4. *The MRI performed 3 months after surgery demonstrated that the tumor was totally removed and the optic radiation was well preserved (**A**, axial image; **B**, sagittal image; **C**, coronal image). The optic cortex can be activated well (red in **A** and **D**).*

or residual tumor, and the surgeon could decide whether to continue with the resection. The surgeons all agreed that without this helpful information they would have been less confident and aggressive in their resection.

There was a discrepancy between the surgeon's estimation of the extent of the resection and the findings of the first iMRI in glioma patients. Of the total discrepant patients, gap $\geq$ 10% occurred in 9 of the 36 cases (25%). However, in the nonglioma group, no discrepancy occurred. This reflected the fact that infiltrative growth of the glioma made it more difficult to resection.

To decrease the intendancy, the surgeon stopped the resection prematurely, for the surgeon believed that there still was tumor, and the iMRI would provide more updated and meaningful information. So, our questionnaire was specifically designed to ask the surgeon to indicate what percentage of the lesion had been resected before the iMRI scan, hopefully minimizing this potential bias. Our data demonstrated that the surgeons tended to overestimate the extent of the resection in glioma patients.

A few published reports have concluded that iMRI-guided surgery increases the extent and rate of resection of cerebral lesions.[61-64] Our findings demonstrated that for the glioma patients, with the help of iMRI and functional neuronavigation, the gross total resection rate increased from 44.4% to 66.7% ($P < .05$) and that the average extent of resection increased from 85.7% to 94.7 % ($P < .01$) with additional tumor removal. For the nonglioma patients, the first iMRI demonstrated the total lesion removal. For the 17 patients who underwent at least 2 iMRI scans, the repeat iMRI scan enabled an increase in the average extent of resection

(first and last iMRI scanning, 74.5% vs 93.3%; $P < .01$). Intraoperative MRI and integrated neuronavigation contributed to increasing the extent of the resection and to the achievement of total removal of the tumor, especially in glioma patients. All residual optic radiation–related tumors were in the lesion to optic radiation < 5 mm group, except 2 that were in the > 5 mm group. One patient (patient 19) did not achieve total removal because the intraoperative reconstructed optic radiation shifted toward the lesion, and total removal of the lesion may have led to visual field deterioration; another patient (patient 40) did not have full resection because the lesion was close to other eloquent areas, and aggressive resection would have caused new neurological deficit.

Does further resection increase the possibility of visual field defects? From our study, contrary to the group who did not undergo further resection, the group who did undergo additional resection did not show a greater tendency to develop visual field defects ($P > .05$). That meant the iMRI and updated neuronavigation could improve the extent of resection while protecting the visual fields. We found that the iMRI was most helpful in low-grade glioma patients in whom the number of repeat iMRI was higher than in the high-grade glioma group. Of the 17 patients who received at least 2 scans, 12 patients were diagnosed with low-grade glioma, and 3 underwent intraoperative scanning 3 times. Low-grade gliomas may not have a well-defined edge or margin. It is nearly impossible to distinguish the lesion from the peripheral normal brain with the naked eye. Therefore, it is very difficult for the surgeon to remove the lesion completely, especially when it is adjacent to the eloquent area. Moreover, brain shift during an operation can make tumor resection more difficult. Thus, iMRI and neuronavigation make it easier and safer for the surgeon to resect the lesion.

In patients with lesions involving the optic radiation, surgical removal of the lesion without fiber tract damage and subsequent visual filed deterioration remains a challenge. The optic radiation is not visible on conventional MRIs, although some authors have reported that it can sometimes be seen on T2-weighted images owing to a low axonal density in the external sagittal stratum.[65,66] Several authors have used DTI techniques based on the fractional anisotrophy map to visualize the optic radiation.[67,68] However, during surgery, the neurosurgeon still has to rely on his or her imaginative capability to locate the optic radiation. With the guidance of functional neuronavigation, the lesion and optic radiation can be seen vividly in 3D under the microscope, and the surgeon can choose a suitable approach to the lesion. With

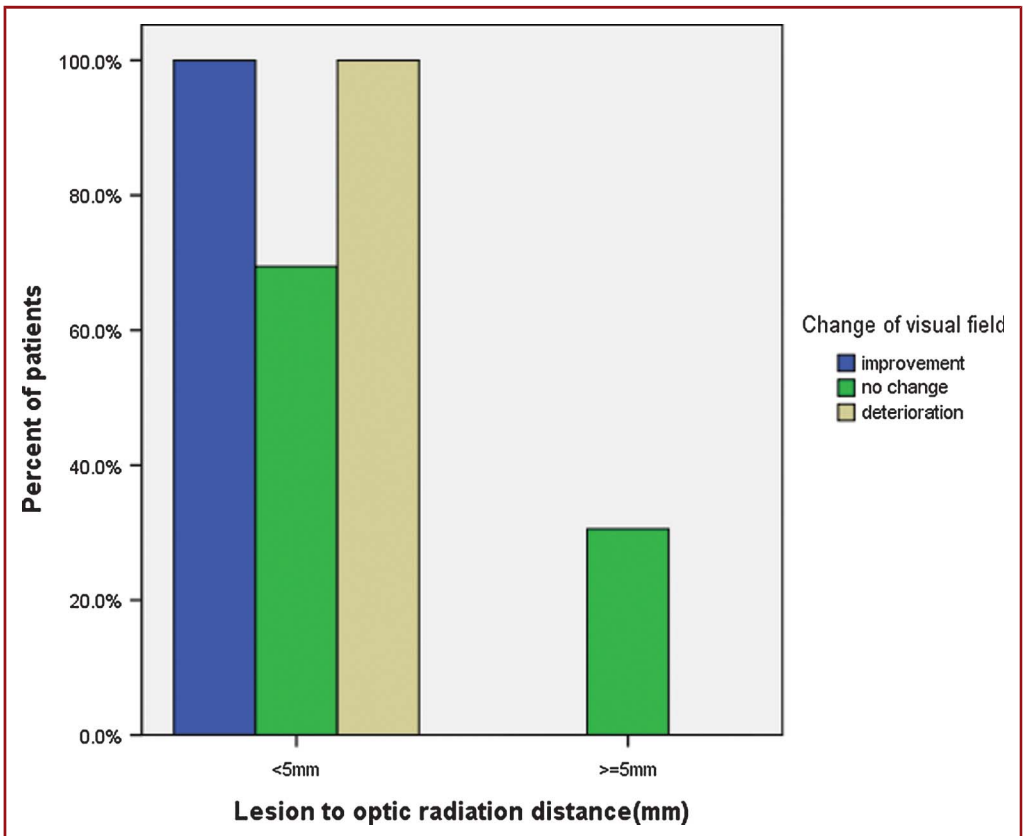

FIGURE 5. *Bar graph demonstrating the postoperative change of the visual field related to the different lesion to optic radiation distance groups. All of the deteriorated patients were in the < 5 mm group. Decreasing the lesion to optic radiation distance was a negative factor for the visual field preservation (P < .05).*

intraoperative imaging, the neuronavigation can be updated timely, and any shift in the location of the optic radiation resulting from brain movement can be corrected. Thus, the operator can visualize the real site that he or she is manipulating, as well as the distance of the resection edge from the optic radiation.

In our study, the visual fields of 41 of the 44 patients (93.2%) were unchanged or improved. In the 8 nonglioma patients, even with the gross total removal of the lesion, no patient had deteriorated visual field. The nonglioma (arteriovenous malformation, cavernous hemangioma, metastatic tumor) often has a relatively clear margin, and the fiber tract adjacent to the lesion can often be displaced instead of infiltrated or destructed. Thus, for the nonglioma patients, it was easy to get high rates of gross total tumor removal and optic radiation preservation. In the glioma patients, the glioma tended to infiltrate the white matter diffusely; there was no clear margin between the adjacent eloquent white matter and the tumor, which made the peritumoral eloquent white matter preservation more difficult. The 3 patients with aggravated visual fields were glioma patients (2 with high-grade gliomas and 1 with a low-grade glioma) in the group of $<$ 5-mm distance between the lesion and the optic radiation (Figure 5).

We also found that when the preoperative reconstructed optic radiation was noticeably stretched and located laterally adjacent to the lesion, the visual field preservation was more difficult.

The patients were divided into an optic radiation stretched or unstretched group. All patients who demonstrated deterioration of visual fields were in the optic radiation stretched group (Figure 6). What was the reason for the deterioration in the visual field when the optic radiation was stretched? First, in our opinion, the optic radiation was compressed by the lesion owing to stretching. Compression of the optic radiation makes it more vulnerable to damage, and there was repeated compression during the surgical procedure. Second, stretching of the optic radiation will decrease during the resection, so the optic radiation may shift in the direction of the manipulation. These factors will decrease the possibility of achieving optimal tract preservation. All patients who had aggravated visual fields were in the lateral location group (Figure 7). Why is lateral localization of a lesion also a negative factor in protecting the optic radiation? As reported in the literature, the thickness of the optic radiation is $<$ 5 mm and its width is 15 to 30 mm.[65,69,70] It is a thin "sheet" extending along the lateral wall of the lateral ventricle. Thus, when the lesion or the

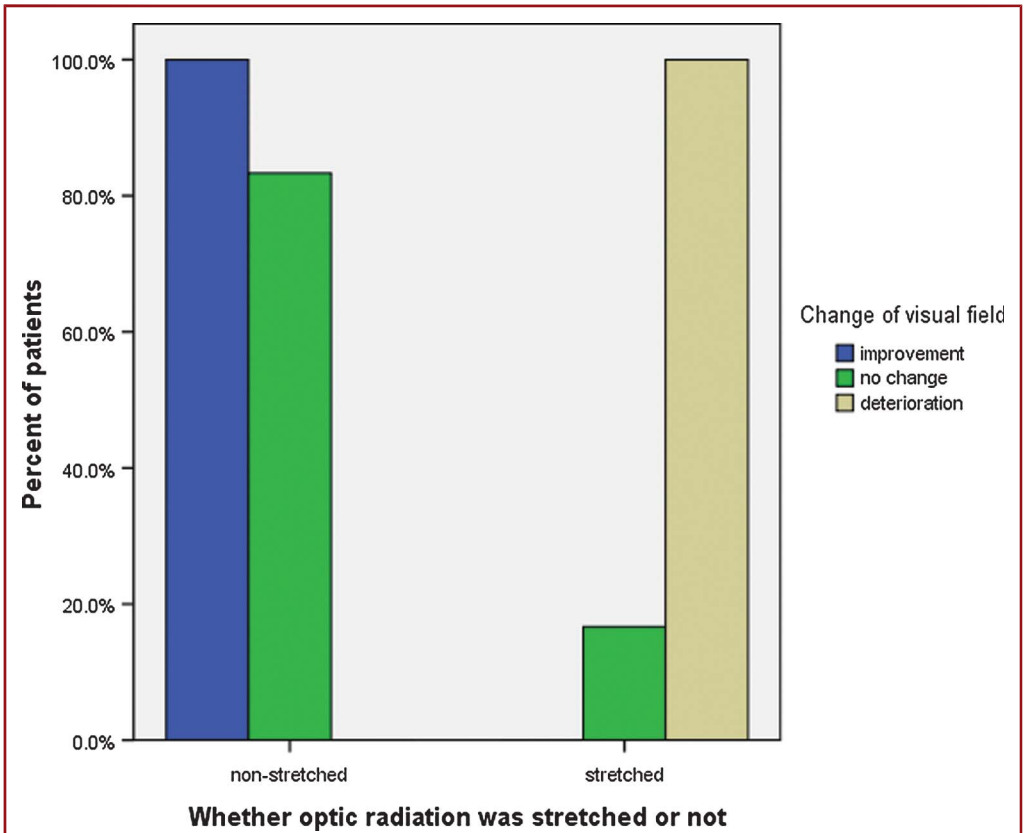

FIGURE 6. *Bar graph demonstrating the postoperative change in the visual field related to whether the optic radiation was stretched by the lesion. All deteriorated patients were in the stretched group. Visual field deterioration was significantly correlated to stretched optic radiation (P $<$ .01).*

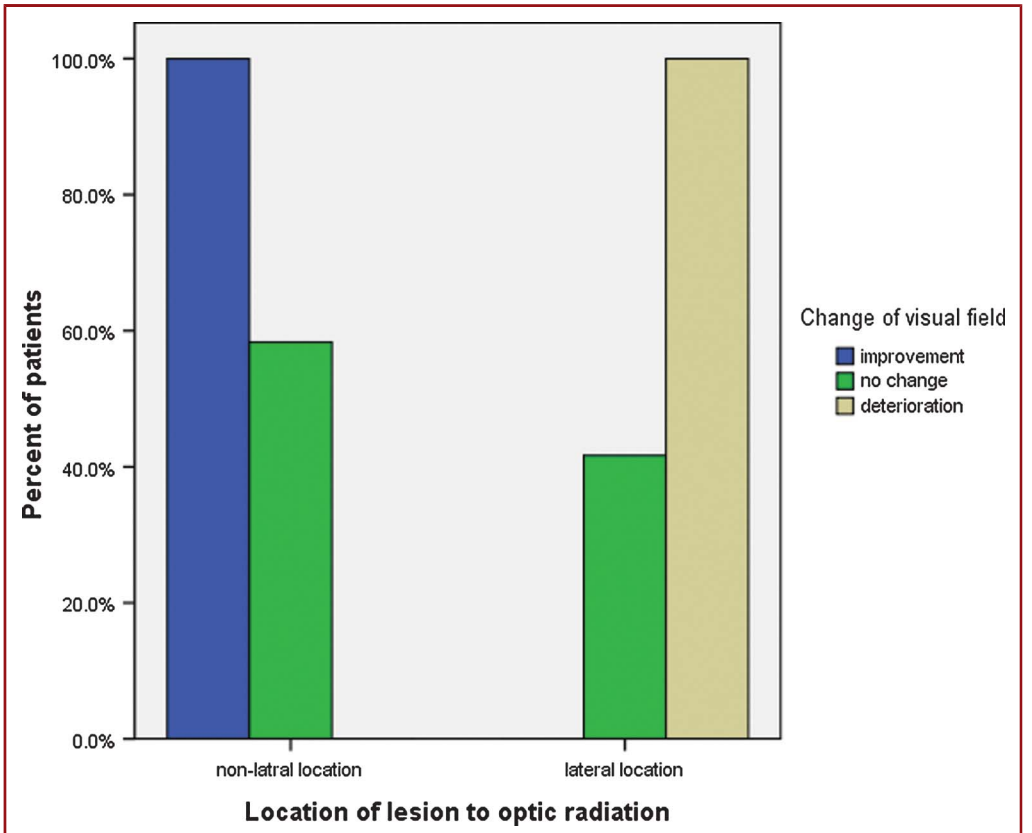

FIGURE 7. *Bar graph demonstrating the postoperative change of the visual field related to whether the lesion was located lateral to the optic radiation. All the deteriorated patients were in the lateral location group. Visual field deterioration was significantly correlated to the lateral location (P < .01).*

manipulation occurs laterally in proximity to the optic radiation, there is a high possibility of damaging this thin structure, and it is easy to induce hemianopia. Our findings showed that, both preoperatively and postoperatively, the majority of the hemianopia occurred where the lesion was located laterally. A similar observation has also been made in another recent study.[71] When the lesion or manipulation is close to the rostral or caudal part of the optic radiation, it is easy to cause upper or lower quadrantanopia. As mentioned, the width of the optic radiation can reach about 30 mm. Thus, a lesion or a manipulation above or below the optic radiation tends to cause partial damage, and quadrantanopia subsequently occurs. The causes of the visual field defects seen in our study agree with the classic theory.

What measures could be taken to avoid optic radiation destruction? First, we could create a 5-mm hull for the reconstructed optic radiation. When the dotted line delineating the hull in the microscope turns into a solid line, the surgeon is reminded that the manipulation is close to the optic radiation and that an iMRI scan is necessary to update the neuronavigation. Second, it is necessary to update the neuronavigation in a timely manner, especially in cases when the optic radiation is stretched, and to correct for a shift in the brain and optic radiation during surgery. Finally, it is important to avoid compression of the optic radiation by surgical manipulation during intratumoral decompression, and dissecting the tumor boundaries from the optic radiation can never be considered too careful. Sometimes, to maintain the optic radiation, we had to leave some residual lesion in the brain.

One limitation of our study is that the cohort investigated was too small to definitively demonstrate the effects of iMRI and functional neuronavigation in terms of improved clinical outcome. A larger cohort in a randomized controlled trial is needed to evaluate the real role of fiber navigation for the resection of lesions involving optic radiation.

CONCLUSION

Preoperative surgical planning based on DTI findings facilitated optimization of the surgical approach. For improved protection of the optic radiation, an iMRI scan should be performed and the neuronavigation updated in a timely manner. Additionally, the manipulation should be carried out lightly and softly.

Intraoperative MRI combined with neuronavigation can help improve tumor removal while preserving the integrity of the optic radiation in most cases.

Disclosures

This work was supported by the National Natural Science Foundation of China (No. 30800349 and No. 31040039). The authors have no personal, financial, or institutional interest in any of the drugs, materials, or devices described in this article.

REFERENCES

1. Ture U, Yasargil MG, Friedman AH, Al-Mefty O. Fiber dissection technique: lateral aspect of the brain. *Neurosurgery*. 2000;47(2):417-427.
2. Coppens JR, Mahaney KB, Abdulrauf SI. An anteromedial approach to the temporal horn to avoid injury to the optic radiation fibers and uncinate fasciculus: anatomical and technical note. *Neurosurg Focus*. 2005;18(6B):E3.
3. Rubino PA, Rhoton AL Jr, Tong X, Oliveira E. Three-dimensional relationships of the optic radiation. *Neurosurgery*. 2005; 57(4)(suppl):219-227.
4. Nagata S, Sasaki T. Lateral transsulcal approach to asymptomatic trigonal meningiomas with correlative microsurgical anatomy: technical case report. *Neurosurgery*. 2005; 56(2)(suppl):E438.
5. Vajkoczy P, Krakow K, Stodieck S, Pohlmann-Eden B, Schmiedek P. Modified approach for the selective treatment of temporal lobe epilepsy: transsylvian-transcisternal mesial en bloc resection. *J Neurosurg*. 1998;88(5):855-862.
6. Ebeling U, Reulen HJ. Neurosurgical topography of the optic radiation in the temporal lobe. *Acta Neurochir (Wien)*. 1988;92(1-4):29-36.
7. Nimsky C, Ganslandt O, Fahlbusch R. Implementation of fiber tract navigation. *Neurosurgery*. 2007;61(1)(suppl):306-318.
8. Peuskens D, van Loon J, Van Calenbergh F, van den Bergh R, Goffin J, Plets C. Anatomy of the anterior temporal lobe and the frontotemporal region demonstrated by fiber dissection. *Neurosurgery*. 2004;55(5):1174-1184.
9. Romano A, D'Andrea G, Minniti G, et al. Pre-surgical planning and MR-tractography utility in brain tumour resection. *Eur Radiol*. 2009;19(12):2798-2808.
10. Jaermann T, De Zanche N, Staempfli P, et al. Preliminary experience with visualization of intracortical fibers by focused high-resolution diffusion tensor imaging. *AJNR Am J Neuroradiol*. 2008;29(1):146-150.
11. Yamamoto A, Miki Y, Urayama S, et al. Diffusion tensor fiber tractography of the optic radiation: analysis with 6-, 12-, 40-, and 81-directional motion-probing gradients, a preliminary study. *AJNR Am J Neuroradiol*. 2007;28(1):92-96.
12. Sherbondy AJ, Dougherty RF, Napel S, Wandell BA. Identifying the human optic radiation using diffusion imaging and fiber tractography. *J Vis*. 2008;8(10):12.1-11.
13. Nilsson D, Starck G, Ljungberg M, et al. Intersubject variability in the anterior extent of the optic radiation assessed by tractography. *Epilepsy Res*. 2007;77(1):11-16.
14. Mori S, Oishi K, Faria AV. White matter atlases based on diffusion tensor imaging. *Curr Opin Neurol*. 2009;22(4):362-369.
15. Basser PJ, Mattiello J, LeBihan D. MR diffusion tensor spectroscopy and imaging. *Biophys J*. 1994;66(1):259-267.
16. Assaf Y, Pasternak O. Diffusion tensor imaging (DTI)-based white matter mapping in brain research: a review. *J Mol Neurosci*. 2008;34(1):51-61.
17. Mori S, Zhang J. Principles of diffusion tensor imaging and its applications to basic neuroscience research. *Neuron*. 2006;51(5):527-539.
18. Liu C, Bammer R, Kim DH, Moseley ME. Self-navigated interleaved spiral (SNAILS): application to high-resolution diffusion tensor imaging. *Magn Reson Med*. 2004;52(6):1388-1396.
19. Giannelli M, Cosottini M, Michelassi MC, et al. Dependence of brain DTI maps of fractional anisotropy and mean diffusivity on the number of diffusion weighting directions. *J Appl Clin Med Phys*. 2010;11(1):2927.
20. Landman BA, Farrell JA, Jones CK, Smith SA, Prince JL, Mori S. Effects of diffusion weighting schemes on the reproducibility of DTI-derived fractional anisotropy, mean diffusivity, and principal eigenvector measurements at 1.5T. *Neuroimage*. 2007;36(4):1123-1138.
21. Nana R, Zhao T, Hu X. Single-shot multiecho parallel echo-planar imaging (EPI) for diffusion tensor imaging (DTI) with improved signal-to-noise ratio (SNR) and reduced distortion. *Magn Reson Med*. 2008;60(6):1512-1517.
22. Jianu R, Demiralp C, Laidlaw DH. Exploring 3D DTI fiber tracts with linked 2D representations. *IEEE Trans Vis Comput Graph*. 2009;15(6):1449-1456.
23. Chen W, Ding Z, Zhang S, et al. A novel interface for interactive exploration of DTI fibers. *IEEE Trans Vis Comput Graph*. 2009;15(6):1433-1440.
24. Kovanlikaya I, Firat Z, Kovanlikaya A, et al. Assessment of the corticospinal tract alterations before and after resection of brainstem lesions using diffusion tensor imaging (DTI) and tractography at 3T. *Eur J Radiol*. 2011;77(3):383-391.
25. Jissendi P, Baudry S, Baleriaux D. Diffusion tensor imaging (DTI) and tractography of the cerebellar projections to prefrontal and posterior parietal cortices: a study at 3T. *J Neuroradiol*. 2008;35(1):42-50.
26. Mori S, van Zijl PC. Fiber tracking: principles and strategies: a technical review. *NMR Biomed*. 2002;15(7-8):468-480.
27. Chen X, Weigel D, Ganslandt O, Fahlbusch R, Buchfelder M, Nimsky C. Diffusion tensor-based fiber tracking and intraoperative neuronavigation for the resection of a brainstem cavernous angioma. *Surg Neurol*. 2007;68(3):285-291.
28. Basser PJ, Pajevic S, Pierpaoli C, Duda J, Aldroubi A. In vivo fiber tractography using DT-MRI data. *Magn Reson Med*. 2000;44(4):625-632.
29. Voineskos AN, O'Donnell LJ, Lobaugh NJ, et al. Quantitative examination of a novel clustering method using magnetic resonance diffusion tensor tractography. *Neuroimage*. 2009;45(2):370-376.
30. Westin CF, Maier SE, Mamata H, Nabavi A, Jolesz FA, Kikinis R. Processing and visualization for diffusion tensor MRI. *Med Image Anal*. 2002;6(2):93-108.
31. Yamamoto T, Yamada K, Nishimura T, Kinoshita S. Tractography to depict three layers of visual field trajectories to the calcarine gyri. *Am J Ophthalmol*. 2005;140(5):781-785.
32. Chen X, Weigel D, Ganslandt O, Buchfelder M, Nimsky C. Prediction of visual field deficits by diffusion tensor imaging in temporal lobe epilepsy surgery. *Neuroimage*. 2009;45(2):286-297.
33. Coenen VA, Huber KK, Krings T, Weidemann J, Gilsbach JM, Rohde V. Diffusion-weighted imaging-guided resection of intracerebral lesions involving the optic radiation. *Neurosurg Rev*. 2005;28(3):188-195.
34. Kamada K, Todo T, Morita A, et al. Functional monitoring for visual pathway using real-time visual evoked potentials and optic-radiation tractography. *Neurosurgery*. 2005;57(1)(Suppl):121-127.
35. Duffau H, Velut S, Mitchell MC, Gatignol P, Capelle L. Intra-operative mapping of the subcortical visual pathways using direct electrical stimulations. *Acta Neurochir (Wien)*. 2004;146(3):265-270.
36. Zhao J, Wang Y, Kang S, et al. The benefit of neuronavigation for the treatment of patients with intracerebral cavernous malformations. *Neurosurg Rev*. 2007;30(4):313-319.
37. Kikuta K, Takagi Y, Nozaki K, et al. Early experience with 3-T magnetic resonance tractography in the surgery of cerebral arteriovenous malformations in and around the visual pathway. *Neurosurgery*. 2006,58(2):331-337.
38. Gasser T, Ganslandt O, Sandalcioglu E, Stolke D, Fahlbusch R, Nimsky C. Intraoperative functional MRI: implementation and preliminary experience. *Neuroimage*. 2005;26(3):685-693.
39. Nimsky C, Ganslandt O, Buchfelder M, Fahlbusch R. Intraoperative visualization for resection of gliomas: the role of functional neuronavigation and intraoperative 1.5 T MRI. *Neurol Res*. 2006;28(5):482-487.
40. Nimsky C, Ganslandt O, von Keller B, Fahlbusch R. Preliminary experience in glioma surgery with intraoperative high-field MRI. *Acta Neurochir Suppl*. 2003;88:21-29.
41. Kubicki M, McCarley R, Westin CF, et al. A review of diffusion tensor imaging studies in schizophrenia. *J Psychiatr Res*. 2007;41(1-2):15-30.
42. Sundgren PC, Dong Q, Gomez-Hassan D, Mukherji SK, Maly P, Welsh R. Diffusion tensor imaging of the brain: review of clinical applications. *Neuroradiology*. 2004;46(5):339-350.
43. Miller JH, McKinstry RC, Philip JV, Mukherjee P, Neil JJ. Diffusion-tensor MR imaging of normal brain maturation: a guide to structural development and myelination. *AJR Am J Roentgenol*. 2003;180(3):851-859.
44. Mukherjee P, McKinstry RC. Diffusion tensor imaging and tractography of human brain development. *Neuroimaging Clin N Am*. 2006;16(1):19-43, vii.
45. Kunimatsu A, Aoki S, Masutani Y, Abe O, Mori H, Ohtomo K. Three-dimensional white matter tractography by diffusion tensor imaging in ischaemic stroke involving the corticospinal tract. *Neuroradiology*. 2003;45(8):532-535.
46. Masutani Y, Aoki S, Abe O, Hayashi N, Otomo K. MR diffusion tensor imaging: recent advance and new techniques for diffusion tensor visualization. *Eur J Radiol*. 2003;46(1):53-66.

47. Okada T, Miki Y, Kikuta K, et al. Diffusion tensor fiber tractography for arteriovenous malformations: quantitative analyses to evaluate the corticospinal tract and optic radiation. *AJNR Am J Neuroradiol*. 2007,28(6):1107-1113.
48. Clark CA, Barrick TR, Murphy MM, Bell BA. White matter fiber tracking in patients with space-occupying lesions of the brain: a new technique for neurosurgical planning? *Neuroimage*. 2003;20(3):1601-1608.
49. Nimsky C, Ganslandt O, Hastreiter P, et al. Preoperative and intraoperative diffusion tensor imaging-based fiber tracking in glioma surgery. *Neurosurgery*. 2007;61(1)(suppl):178-186.
50. Krings T, Reinges MH, Thiex R, Gilsbach JM, Thron A. Functional and diffusion-weighted magnetic resonance images of space-occupying lesions affecting the motor system: imaging the motor cortex and pyramidal tracts. *J Neurosurg*. 2001;95(5):816-824.
51. Nimsky C, Ganslandt O, Merhof D, Sorensen AG, Fahlbusch R. Intraoperative visualization of the pyramidal tract by diffusion-tensor-imaging-based fiber tracking. *Neuroimage*. 2006;30(4):1219-1229.
52. Yu CS, Li KC, Xuan Y, Ji XM, Qin W. Diffusion tensor tractography in patients with cerebral tumors: a helpful technique for neurosurgical planning and postoperative assessment. *Eur J Radiol*. 2005;56(2):197-204.
53. Mikuni N, Okada T, Enatsu R, et al. Clinical significance of preoperative fibre-tracking to preserve the affected pyramidal tracts during resection of brain tumours in patients with preoperative motor weakness. *J Neurol Neurosurg Psychiatry*. 2007,78(7):716-721.
54. Nimsky C, Grummich P, Sorensen AG, Fahlbusch R, Ganslandt O. Visualization of the pyramidal tract in glioma surgery by integrating diffusion tensor imaging in functional neuronavigation. *Zentralbl Neurochir*. 2005;66(3):133-141.
55. Okada T, Mikuni N, Miki Y, et al. Corticospinal tract localization: integration of diffusion-tensor tractography at 3-T MR imaging with intraoperative white matter stimulation mapping: preliminary results. *Radiology*. 2006ZCOM-MAZ240(3):849-857.
56. Coenen VA, Krings T, Mayfrank L, et al. Three-dimensional visualization of the pyramidal tract in a neuronavigation system during brain tumor surgery: first experiences and technical note. *Neurosurgery*. 2001;49(1):86-93.
57. Keles GE. Intracranial neuronavigation with intraoperative magnetic resonance imaging. *Curr Opin Neurol*. 2004;17(4):497-500.
58. Nimsky C, Ganslandt O, Kober H, et al. Integration of functional magnetic resonance imaging supported by magnetoencephalography in functional neuronavigation. *Neurosurgery*. 1999;44(6):1249-1256.
59. Brinker T, Arango G, Kaminsky J, et al. An experimental approach to image guided skull base surgery employing a microscope-based neuronavigation system. *Acta Neurochir (Wien)*. 1998;140(9):883-889.
60. Nimsky C, Ganslandt O, Kober H, Buchfelder M, Fahlbusch R. Intraoperative magnetic resonance imaging combined with neuronavigation: a new concept. *Neurosurgery*. 2001;48(5):1082-1091.
61. Bradley WG. Achieving gross total resection of brain tumors: intraoperative MR imaging can make a big difference. *AJNR Am J Neuroradiol*. 2002;23(3):348-349.
62. Bohinski RJ, Warnick RE, Gaskill-Shipley MF, et al. Intraoperative magnetic resonance imaging to determine the extent of resection of pituitary macroadenomas during transsphenoidal microsurgery. *Neurosurgery*. 2001;49(5):1133-1144.
63. Muragaki Y, Iseki H, Maruyama T, et al. Usefulness of intraoperative magnetic resonance imaging for glioma surgery. *Acta Neurochir Suppl*. 2006;98:67-75.
64. Ramina R, Coelho Neto M, Giacomelli A, et al. Optimizing costs of intraoperative magnetic resonance imaging: a series of 29 glioma cases. *Acta Neurochir (Wien)*. 2010;152(1):27-33.
65. Kitajima M, Korogi Y, Takahashi M, Eto K. MR signal intensity of the optic radiation. *AJNR Am J Neuroradiol*. 1996;17(7):1379-1783.
66. Hosoya T, Adachi M, Yamaguchi K, Haku T. MRI anatomy of white matter layers around the trigone of the lateral ventricle. *Neuroradiology*. 1998;40(8):477-482.
67. Ciccarelli O, Toosy AT, Hickman SJ, et al. Optic radiation changes after optic neuritis detected by tractography-based group mapping. *Hum Brain Mapp*. 2005;25(3):308-316.
68. Ciccarelli O, Parker GJ, Toosy AT, et al. From diffusion tractography to quantitative white matter tract measures: a reproducibility study. *Neuroimage*. 2003;18(2):348-359.
69. Mori N, Miki Y, Kasahara S, et al. Susceptibility-weighted imaging at 3 Tesla delineates the optic radiation. *Invest Radiol*. 2009;44(3):140-145.
70. Jolesz FA, Polak JF, Adams DF, Ruenzel PW. Myelinated and nonmyelinated nerves: comparison of proton MR properties. *Radiology*. 1987;164(1):89-91.
71. Shinoura N, Suzuki Y, Yamada R, Tabei Y, Saito K, Yagi K. Relationships between brain tumor and optic tract or calcarine fissure are involved in visual field deficits after surgery for brain tumor. *Acta Neurochir (Wien)*. 2010;152(4):637-642.

Acknowledgments

We thank the members of the Department of Neurosurgery, PLA General Hospital (Xin-guang Yu, MD, PhD; Jun Zhang, MD; Zheng-Hui Sun, MD; Jin-Li Jiang, MD; Xiao-Dong Ma, MD; Bo-Bu, MD; Ru-Yuan Zhu, MD) for their collaborative support.

COMMENTS

Sun et al performed a thorough prospective clinical study on the impact of intraoperative magnetic resonance imaging with preoperative, intraoperative, and postoperative tractography of the optic radiation on surgical radicality and clinical outcome of the patients. They included 44 patients with highly eloquent lesions adjacent to the optic radiation. Intraoperative visualization of white matter tracts led to improvement of the gross total tumor resection rate in gliomas from 44.4% to 66.7%. The average extent of resection was improved from 85.7% to 94.7%. At the same time, there was no increase in visual field deficits after continued tumor resection. Further interesting findings are the negative influence of fiber tract dislocation and stretching on the patient's functional outcome and the surgeon's overestimation of the surgical radicality.

Functional imaging, clinical evaluation, surgery, and discussion of the results are expertly done. This rather large series of patients with lesions next to eloquent white matter underlines the importance of intraoperative image guidance for a certain subgroup of lesions. Furthermore, it shows the positive effect of updating imaging data intraoperatively to estimate the extent of tumor resection.

Lennart H. Stieglitz
Berne, Switzerland

The authors reconstructed optic radiation fiber tracking in patients with intracranial space-occupying lesions. They examined the usefulness of functional neuronavigation by integration of preoperative fiber tracking, intraoperative magnetic resonance imaging, and intraoperative updating of fiber tracking affected by brain shift. Optic radiation fiber tracking is challenging compared with corticospinal tracking because of its complicated anatomic course, sharp turn, or lower fractional anisotropy in the voxel assigned to the fiber volume. The authors solved various problems regarding the optic radiation fiber tracking, and they established a comprehensive functional neuronavigation system. Although the actual distances between the tumor and fiber trajectories are probably different from those measured on fiber tracking technique, the authors created a 5-mm-thick hull around the fiber tracking as a safety margin, which provided considerable visual preservation results. Their tumor resection rate also increased, and better control of disease while preserving higher visual acuity may be expected.

Tsutomu Okada
Osaka, Japan